JOURNAL OF Applied Polymer SCIENCE

Formation of Polyamide 12 Membranes via Thermal–Nonsolvent Induced Phase Separation

Hsu-Hsien Chang,[1] Konstantinos Beltsios,[2] Dar-Jong Lin,[1,3] Liao-Ping Cheng[1,3]

[1]Department of Chemical and Materials Engineering, Tamkang University, New Taipei City, Taiwan
[2]Department of Materials Science and Engineering, University of Ioannina, Ioannina, Greece
[3]Energy and Opto-Electronic Materials Research Center, Tamkang University, New Taipei City, Taiwan
Correspondence to: L.-P. Cheng (E-mail: lpcheng@mail.tku.edu.tw)

ABSTRACT: The thermal–nonsolvent induced phase separation method was used for the fabrication of porous membranes from polyamide 12 (PA12), an attractive engineering polymer; the water/formic acid (FA)/PA12 ternary system is explored in detail. Scanning electron microscopy, differential scanning calorimetry, X-ray diffractometry, tensile strength analysis, and water flux were used to characterize the structure and properties of the fabricated membranes. The morphology of the membranes was found to depend on the FA content in the bath. The top surface of the membrane becomes less dense with increasing FA content in the bath. The cross section and bottom surface of all membranes exhibited a cellular morphology, except for the case of the novel procedure of dope precipitation in a cold neat solvent (FA) bath. In all cases membranes exhibited a crystallinity of ca. 38% with a melting point of ca. 179°C; tensile strengths in excess of 10 MPa were found possible in some cases. © 2013 Wiley Periodicals, Inc. J. Appl. Polym. Sci. 130: 14–24, 2013

KEYWORDS: PA12; phase inversion; TNIPS; morphology; membrane casting

Received 19 September 2012; accepted 4 February 2013; published online 2 March 2013
DOI: 10.1002/app.39138

INTRODUCTION

Polyamide 12 (PA12) is a polymer having properties between those of common nylons (e.g., PA6 and PA66) and polyethylene because of the reduced frequency of amide sites along the chain. In particular, PA12 is characterized by low moisture absorption and low density (compared to that of PA6 and PA66), accompanied by chemical resistance similar to that of PA6 yet exhibiting lower sensitivity to stress cracking. Furthermore, PA12 shows excellent impact strength and Young's modulus values substantially higher than those of various polyethylenes, for additional features of PA12 and comparisons with other polymers (see, for example, Ref. [1]) In view of properties such as the aforementioned ones, PA12 is an attractive engineering plastic already finding various technical applications, while new applications appear possible in the near future. Therefore, it is interesting to consider PA12 as a framework material for porous polymeric membranes.

It is worth noting that polyolefins are cast into the form of porous membranes via phase separation mostly by the thermally induced phase separation (TIPS) method.[2–6] In this case, the formed membranes exhibit largely zero or at best very mild asymmetry.[7,8] This is because heat transfer involved in TIPS is much faster than the mass transfer involved in wet phase inversion (also known as nonsolvent induced phase separation, NIPS).[9–13] On the other hand common nylons (such as PA6 and PA66) have been explored systematically so far as regards their potential for both symmetric and asymmetric membrane formation.[14–17] The difference is largely due to the fact that semicrystalline polyolefins cannot form concentrated solutions at room temperature (or somewhat higher), and hence, the technically more demanding TIPS approach is adopted.[18–20] In contrast, semicrystalline polyamides dissolve more easily (in appropriate solvents), and hence, they are largely explored as regards their NIPS potential.

Here, we study the porous membrane potential of PA12, and we opt to apply the thermal–nonsolvent induced phase separation (TNIPS) process,[21] i.e., the combination of NIPS with a thermal quench, which is a processing approach more versatile than either NIPS or TIPS alone. In terms of a pseudo-binary description, the TNIPS method used for membrane preparation amounts to polymer precipitation through increase of the χ parameter (Flory–Huggins interaction parameter) in two ways, namely, temperature lowering and enhancement of the nonsolvent content of the casting solution. The increase of χ

parameter favors both polymer crystallization and liquid–liquid phase separation. As expected,[22] proper tuning of TNIPS parameters is capable of leading to both symmetric and asymmetric porous structures.

Microporous PA12 membranes with different porous morphologies were prepared via the TNIPS method. The effects of coagulation bath temperature and composition harshness are studied in detail; brief consideration of an interesting degenerate case corresponding to the use of pure cold solvent as coagulation bath is included. The structure and performance of the new membranes are studied by a host of techniques [scanning electron microscopy (SEM), differential scanning calorimetry (DSC), X-ray diffractometry (XRD), tensile testing, water permeability]. The results suggest that some of the currently developed membranes may find applications in microfiltration (waste water treatment, sterilization, etc.) processes.

METHODS

Materials

PA12 (Grilamid, L20G, M_n = 24,000) was purchased from Emser Werke, Steinheim, Germany. Formic acid (FA, Aldrich, reagent grade) and distilled and deionized water were used as solvent and nonsolvent for PA12, respectively. All of the materials were used as received.

Phase Diagram Determination

The gelation phase boundaries at 60 and 80°C for the ternary system, water/FA/PA12, was determined by a method described elsewhere.[23,24] Briefly, a specific amount of polymer (dried in an oven at 60°C) was mixed with solvent and sealed in a glass bottle with a Teflon-lined cap. This mixture was blended at 80°C until the polymer was completely dissolved; a known quantity of water was added to the solution formed. Local precipitation was observed, and the mixture was further blended at 80°C until a clear homogeneous solution was again obtained. This solution was then put in a thermostatically controlled thermostat maintained at 60°C or 80°C, respectively, for the period of 30 days. The gelation points were identified as the compositions at which homogeneous solutions began to gel (as a result of polymer crystallization) in a series of samples with different nonsolvent/solvent ratios.

There is also a submerged (i.e., overall metastable) binodal surface; this surface cannot be determined in the same manner as the crystallization surface, but its presence can be inferred from morphological observations suggesting liquid–liquid separation for some of our membrane fabrication experiments (see "Results and discussion" section).

Membrane Preparation and Characterization

PA12 membranes were prepared in the form of flat sheets by the TNIPS method. First, PA12 was dissolved in FA at 80°C on a roller to form a 20 wt % homogeneous solution. This solution was held at 80°C for 1 h and then cast on a glass plate using a casting knife with a clearance of 400 μm. Following casting, the solution was immersed in a coagulation bath held at constant temperature (10, 25, or 40°C) to induce polymer precipitation. The formed nascent membrane was removed from the glass plate and washed in a series of nonsolvents (typically isopropanol, then hexane) in order to extract residual FA. Subsequently, the membrane was press-dried between sheets of filter papers at 50°C. The preparation conditions for various membranes are listed in Table I. The following methods were used to characterize the formed membranes.

Membrane Morphology by SEM. Morphologies of the membranes were observed in the top, bottom, and cross-sectional views using a field emission SEM (Leo 1530, Carl Zeiss, Oberkochen, Germany). A piece of membrane sample was vacuum-dried and then attached to a sample holder by conductive copper tapes. The cross section of the membrane was obtained by fracturing the membrane in liquid nitrogen. Silver paste was applied at the edges of the sample to enhance electronic conductivity. Then, the sample was sputtered with a thin layer (~2 nm) of Pt–Pd alloy and observed under a low acceleration voltage, 2 kV, by means of an in-lens detector.

Structure of PA12 Crystals by WXRD. The structure of PA12 crystals in the membrane was determined by a wide angle X-ray diffractometer (WXRD, D8 Advance, Bruker, Karlsruhe, Germany). The operating parameters were as follows: source intensity = 40 kV/40 mA, λ = 1.54 Å (copper K_α line), source slit width = 0.6 mm, increment = 0.05°/step, scanning speed = 3 s/step, and scanning range = $10° < 2\theta < 30°$. Crystallinity of the sample was determined by deconvolution of the diffraction peaks into amorphous and crystalline contributions, following a curve fitting method described in the literature.[15,23] The curve fitting scheme incorporated Gaussian and Lorenzian functions in a mixed form by means of a commercial software, GRAMS/AI^{TM}.

Thermal Behavior of PA12 Membranes by DSC. The thermal behavior of the prepared membranes was observed using a differential scanning calorimeter (MDSC 2920, TA Instrument, New Castle, DE). The instrument was calibrated with an indium standard before running the tests. An appropriate amount of membrane sample (typically 5–10 mg) was sealed in an aluminum pan and placed in the heating chamber together with an empty pan serving as reference. The temperature was raised from 30 to 200°C at a rate of 10°C/min in a nitrogen atmosphere. The melting temperature (T_m) and the heat of fusion (ΔH_H) were determined from the obtained thermograms. The crystallinity of the membranes was calculated by dividing the measured ΔH_H by the literature value for the heat of fusion of a perfect PA12 crystal (ΔH^0 = 233.6 J/g).[25–27]

Porosity of PA12 Membranes. The porosity of the membrane was determined by the following equation[23,28]:

$$\text{Porosity}(\%) = \left[\frac{(V_m - V_p)}{V_m}\right] \times 100\%,$$

where V_m is the bulk volume of the membrane, and V_V is the volume of the polymer. V_V was obtained by multiplying the membrane area with its thickness, which was measured by a thickness gauge. V_V can be calculated by W_W/ρ_p, where W_W is the weight of the membrane, and ρ_p is the density of polymer. The value of ρ_p = 1.03 g/cm^3 was assumed for PA12.[29]

Tensile Strength and Elongation of PA12 Membranes. The tensile strength and elongation at the breaking point (DaChang, QC-512, Taichung, Taiwan) for various membranes were measured following ASTM (D638 IV).

Pure Water Fluxes of the PA12 Membranes by Dead-End Filtration System. Pure water fluxes of the pre-wet PA12 membranes were measured with a dead-end filtration system (effective area 11.34 cm^2) at 40 kPa pressure. Each of the prepared

Table I. Preparation Conditions[a] and Properties of PA12 Membranes

Bath	Code	Bath temp. (°C)	Thickness (μm)	Porosity[b] (%)	Water flux (LMH | kPa)
Water	MW-10	10	133 ± 3	43.41 ± 1.28	0 | 392
	MW-25	25	133 ± 7	45.02 ± 2.91	0 | 392
	MW-40	40	151 ± 3	54.02 ± 0.91	0 | 392
30 wt % FA	M30-10	10	147 ± 6	46.34 ± 1.59	0 | 392
	M30-25	25	138 ± 5	55.85 ± 1.24	0 | 392
	M30-40	40	147 ± 8	55.49 ± 1.56	0 | 392
50 wt % FA	M50-10	10	146 ± 4	50.60 ± 0.70	0 | 392
	M50-25	25	151 ± 2	54.40 ± 0.33	0 | 392
	M50-40	40	144 ± 5	57.88 ± 1.15	0 | 392
70 wt % FA	M70-10	10	134 ± 4	53.26 ± 1.28	0 | 392
	M70-25	25	143 ± 4	56.76 ± 0.58	0 | 392
	M70-40	40	143 ± 5	56.82 ± 1.50	0 | 392
80 wt % FA	M80-10	10	132 ± 3	54.05 ± 1.88	0 | 392
	M80-25	25	140 ± 1	54.05 ± 1.67	0 | 392
	M80-40	40	147 ± 4	58.31 ± 2.27	0 | 392
90 wt % FA	M90-10	10	153 ± 6	53.31 ± 1.83	0 | 392
	M90-25	25	149 ± 3	56.33 ± 0.88	0 | 392
	M90-40	40	147 ± 2	59.05 ± 0.56	0 | 392
95 wt % FA	M95-10	10	164 ± 4	55.73 ± 1.08	53 ± 25 | 392
	M95-25	25	165 ± 3	57.99 ± 0.77	625 ± 71 | 392
	M95-40	40	156 ± 2	56.59 ± 0.56	39 ± 18 | 392
FA	MFA-10	10	164 ± 6	59.73 ± 0.98	6376 ± 254 | 40
	MFA-25	25[c]	-	-	-
	MFA-40	40[c]	-	-	-

[a]Dope: 20 wt % PA12 in FA at 80°C.
[b]Calculated based on the density of PA12 (1.03 g/cm^3) and the measured mass and thickness of the membrane.
[c]Polymer powder; no coherent membrane was obtained when the *neat* FA bath was kept at 25°C or 40°C.

membranes was wetted for 24 h in ethanol, and then it was soaked for 24 h in water to extract residual ethanol. Subsequently, the membrane was placed in the filtration system, and water flux was measured at ca. 25°C.

Pore Size of the PA12 Membranes by the Bubble-Point Method. For the measurement of the pore size, the bubble-point method was used. PA12 membrane sample was cut into circular shape (3.8 cm in diameter) and wetted by the 2-propanol (IPA) solution first. This solution is a standard wetting medium, for which surface tension is adjusted to 21.7×10^{-3} N/m. Then, the fully wetted sample is placed in the sealed sample chamber. Nitrogen gas is then allowed to flow into the chamber behind the sample. When the pressure reached a point that could overcome the capillary action of the fluid within the largest pore, the bubble point was obtained. The pore radius is calculated according to the following equation[30–32]:

$$r_p = \left(\frac{2\gamma}{P}\right)\cos\theta,$$

where r_r is the pore radius, γ is the surface tension of the wetting solution (IPA: $\gamma = 21.7 \times 10^{-3}$ N/m), θ is the contact angle of wetting solution, and P is the gas pressure.

RESULTS AND DISCUSSION

Phase Diagram of the Water/FA/PA12 System

The experimental phase equilibrium boundaries at 60 and 80°C for the water/FA/PA12 system are shown in Figure 1. The filled circles represent the gelation points for PA12 in water/FA solutions at 60°C. The gelation was actually induced by polymer crystallization, which has been extensively discussed for many nonsolvent–solvent–crystalline polymer systems employed for the preparation of porous membranes.[16,17,23,24] Figure 2 shows the image of a gelled dope (20% polymer in FA) under cross-polarized optical microscope. The Maltese cross pattern verifies undoubtedly the presence of spherulites of ~10 μm in the gel. A curve connecting the experimentally determined gelation points formed the gelation line (or crystallization line) for each temperature. To the left of the gelation line is a one-phase region, in which a homogeneous casting dope can be prepared with long-term stability. To the right of the gelation line is a metastable zone, in which an originally uniform dope solution will gel upon standing at 60°C over an extended period of time. As the temperature is raised, gels that are formed at lower temperatures may gain enough thermal energy to turn into homogeneous solutions. Hence, the gelation boundary shifts

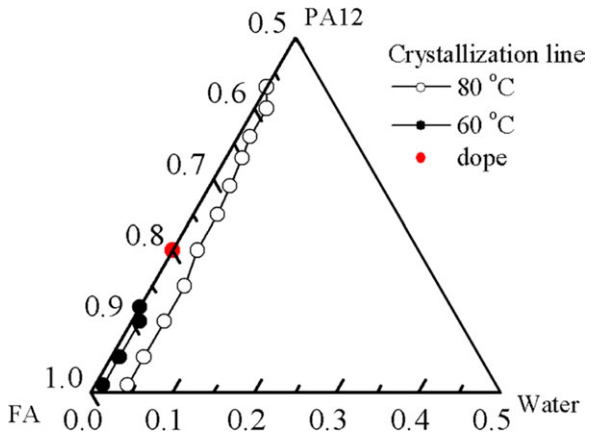

Figure 1. Phase diagram of the water/FA/PA12 system. [Color figure can be viewed in the online issue, which is available at wileyonlinelibrary.com.]

downward with increasing temperature and the one-phase region becomes larger, as shown in Figure 1 for the gelation line measured at 80°C. In other words, gelation can be induced either by enhancement of the nonsolvent content of the solution or by temperature reduction.

Morphologies of PA12 Membranes Formed by TNIPS

PA12 membranes were prepared by immersion-precipitation of the dope having the composition and temperature indicated in Figure 1 in pure water bath or bath containing a certain amount of FA. The dope was held at 80°C prior to immersion, whereas the bath temperature was maintained at 10, 25, or 40°C. The effects of bath temperature and bath concentration on the morphologies of the formed membranes are discussed below.

Effect of FA Concentration in the Precipitation Bath at 25°C. In Figure 3, morphologies of the membrane precipitated from water bath at 25°C are demonstrated. The top surface exhibits the form of a dense nonporous skin, which appears featureless even when observed at a resolution of ~20 nm. In general, skin derives from high interfacial polymer concentration that develops during precipitation in a harsh bath.[17,23,24] As a result, a stiff top layer is produced near the surface, which precludes the nucleation of liquid domains and formation of micropores in this layer. However, as the composition of this layer is within the crystallization region (c.f. Figure 1), crystallization will eventually take place in this stiff top gel layer. The cross-sectional morphology of the membrane is shown in Figure 3(b). The membrane exhibits cellular pores of 1–2 μm size. A porous morphology of the latter type is typically observed when liquid–liquid demixing (via nucleation of polymer-poor droplets) of the casting solution dominates structure formation; polymer crystallization follows, defines fine features, and also stiffens the framework of the membrane. Morphological evidence of crystallization can be observed only in very high magnification images, as in Figure 3(c) which shows the details of pore walls; the walls exhibit a rough texture resulting from open arrangements of crystallites having a thickness in the 20 nm range (a size typical for polymer lamellae and related polymer single crystals).

The morphology of the bottom surface is a thicker-wall variety of the cross-sectional morphology, as shown in Figure 3(d). The cellular pores exhibit little interconnectivity and sizes similar to the size of the pores found in the bulk of the membrane. From the above observation, it can be deduced that, after immersion of the dope in the bath, liquid–liquid demixing initiates, and the liquid phase grows quickly to set-in the cellular structure. Subsequently, the polymer of the polymer-rich phase crystallizes to become the continuous matrix; additional details of the pertinent formation mechanism are described in the literature.[17,33] On the other hand, when the casting solution was quenched directly to 25°C without contacting the bath liquid, i.e., when a neat TIPS processing was applied, pieces of white solid flakes were obtained. As shown in Figure 4, the latter TIPS processing leads to a microstructure consisting of large full spherulites having a 6–20 μm diameter; crystallization has dominated the precipitation process, and liquid–liquid demixing, if any, was only a secondary and/or follow-up process.[34–38] Comparing the TIPS and the TNIPS cases discussed above, it can be inferred that water is such a strong nonsolvent that it induces liquid–liquid demixing very effectively, and the morphological role of crystallization was suppressed despite the presence of a thermal driving force.

The rate of precipitation slows down when a casting dope is immersed in a bath containing substantial amount of solvent (i.e., when a soft precipitation bath is employed); in this case, the concentration gradients for solvent and nonsolvent to diffuse across the membrane–bath interface become smaller. As a result, the casting dope enters the liquid–liquid phase separation boundaries sluggishly, leading to the so-called delayed-type demixing.[15,17,23] Moreover, as the polymer concentration at the membrane–bath interface is relatively low in the soft bath, the gel layer formed near the top surface will be less stiff than that formed in the case of a water bath. As an example, Figure 5

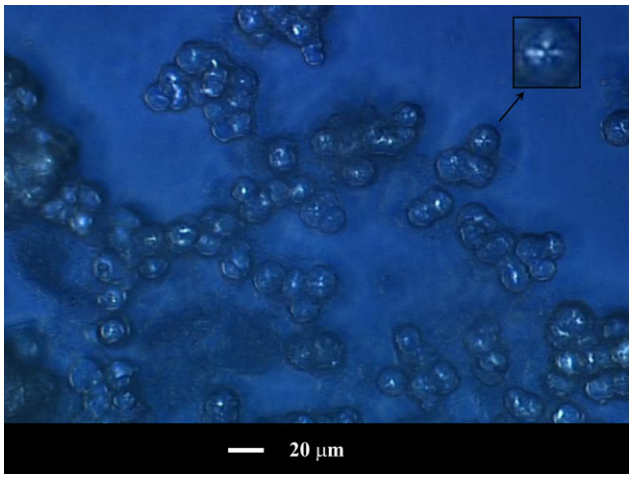

Figure 2. Cross-polarized microscopic image of a crystalline gel. Initial composition of the dope: PA12 20% and FA 80%. [Color figure can be viewed in the online issue, which is available at wileyonlinelibrary.com.]

Applied Polymer SCIENCE

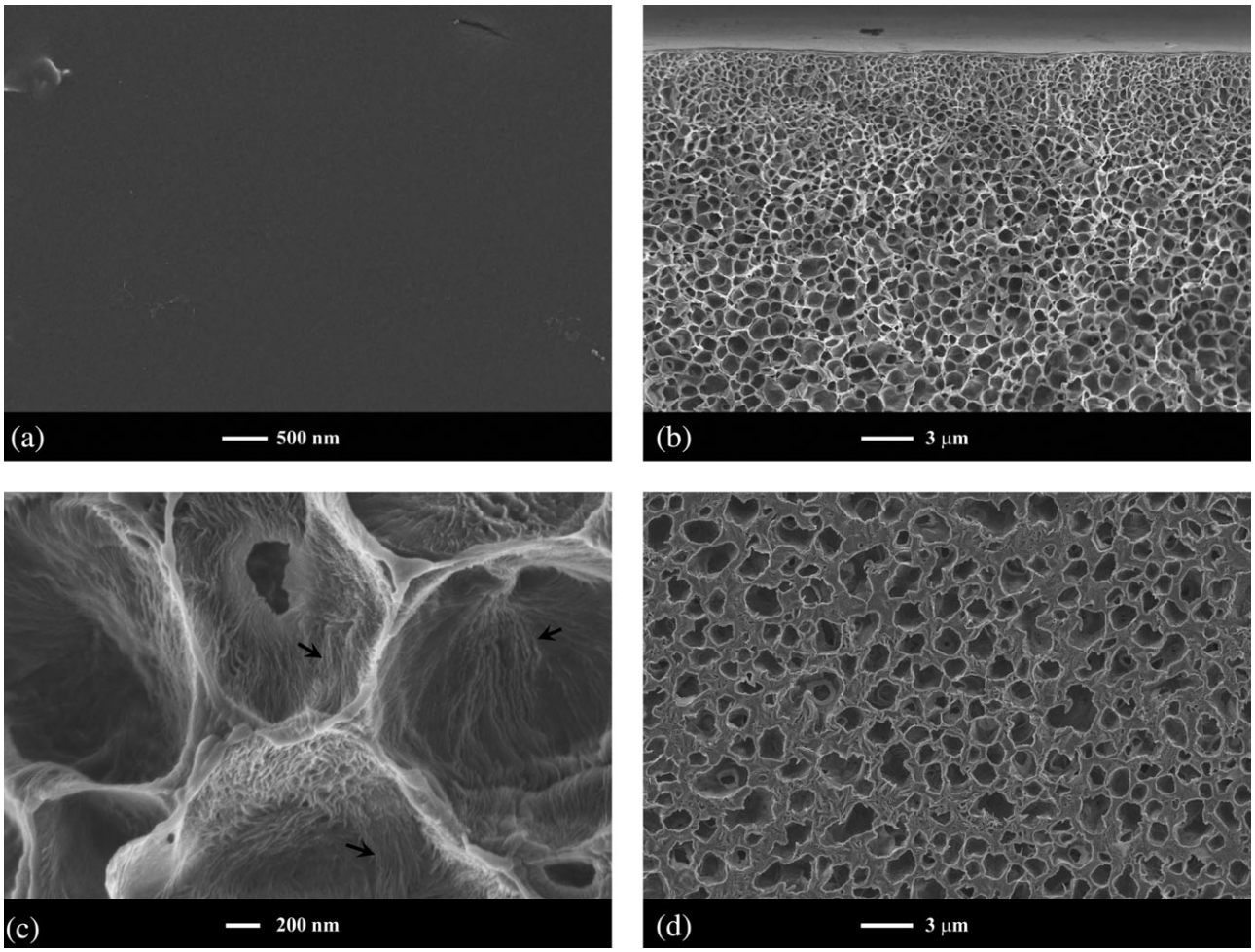

Figure 3. SEM micrographs of the PA12 membrane. Bath: 25°C pure water, Dope: 20 wt % PA12 in FA. (a) Top surface, (b) cross section, (c) high magnification of (b), and (d) bottom surface.

demonstrates the morphologies of the membrane precipitated from a bath containing 90 wt % FA at 25°C. In Figure 5(a), the top surface consists of globular semicrystalline entities (spherulites); a flat side seen in some of the globules reflects growth at the membrane–bath contacting plane. Large crevices are clearly seen between globules. Such a loosely packed skin derives from a weak gel layer, which was easily disrupted by the growing polymer crystallites. The spherulites have similar sizes, and the grain boundaries are linear suggesting that they were nucleated roughly at the same time.

Cross-sectional morphology of the membrane is shown in Figure 5(b). It is of the cellular type, similar to that shown in Figure 3(b). However, the pores here are larger, ~3 μm, implying a lower nucleation density of liquid domains during demixing in this soft bath case; such an effect has been observed previously[16,39] and has been related to lower polymer concentrations.

Effect of the Precipitation Temperature. The effect of precipitation temperature on membrane morphology is evident upon comparison of membrane cross sections. Figure 6 shows the membrane morphologies for the cases of precipitation in 90 wt % FA baths at 10, 25, and 40°C. In the case of the 10°C bath, the pore size of the formed membrane is about 1–2 μm across the cross section, and as the bath temperature is increased, the pore size increases considerably; for example, in the 40°C bath,

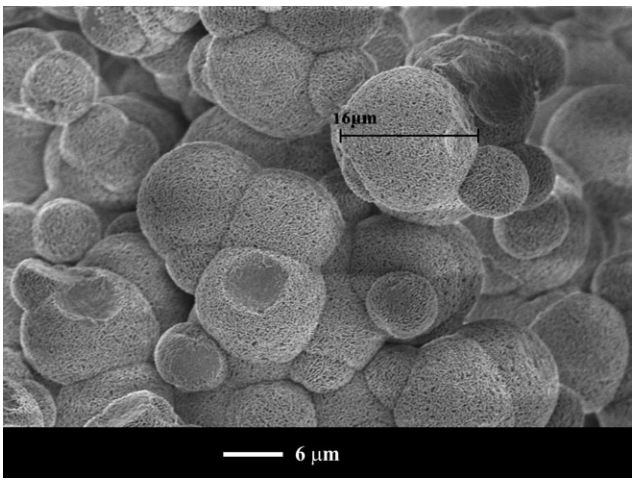

Figure 4. SEM micrographs of the PA12 membrane from the TIPS process at 25°C. Dope: 20 wt % PA12 in FA.

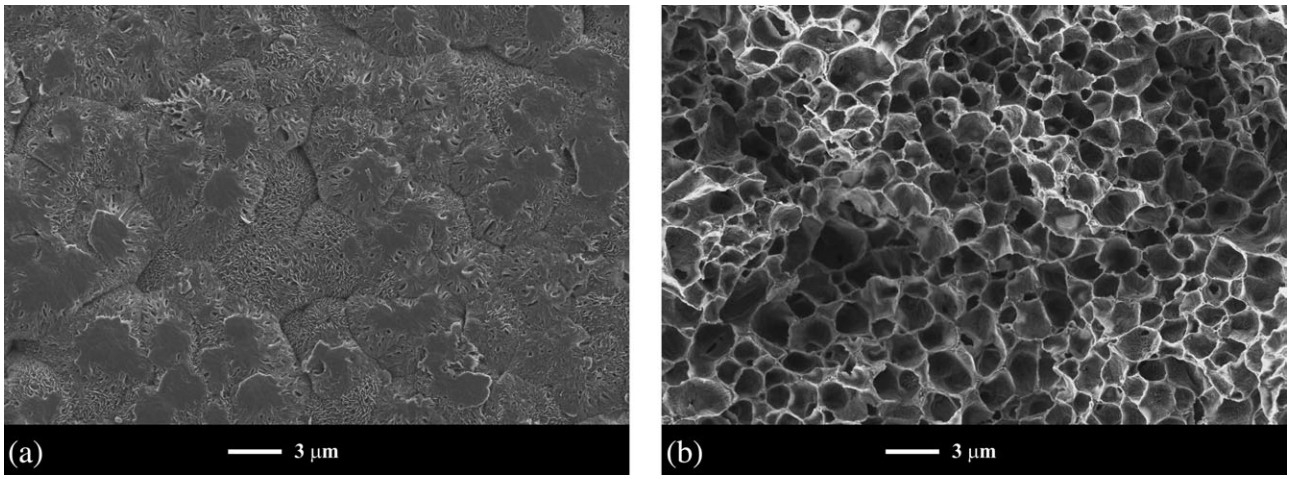

Figure 5. SEM micrographs of the PA12 membrane. Bath: 90 wt % FA at 25°C, Dope: 20 wt % PA12 in FA. (a) Top surface and (b) cross section.

the pores become as large as 5 μm. Hence, it is an experimental fact that our samples exhibit smaller pores for lower quench temperatures; in addition, pore interconnectivity appears to be somewhat more extensive in the case of lower quench temperatures. The factors affecting spacing are numerous and interacting in a complex fashion that precludes safe quantification or even safe prediction of the qualitative trend (as regards pore size as a function of quench temperature); yet we can site some helpful theoretical concepts pertinent to our findings.

In a unified description of liquid–liquid demixing (phase separation within a binodal), the spacing, for isothermal phase separation and before coarsening sets-in, drops continuously as we move from the binodal border to the center of the spinodal subregion.[40] In addition, for a given overall composition, deeper quenches (i.e., quenches that end at temperatures for which the binodal and the spinodal are broader) tend to favor smaller spacings (e.g., Ref. [41]). In our case, neither temperature nor overall composition are fixed during structure formation, but if we consider qualitatively both of the aforementioned factors, we might attribute the smaller spacing for lower bath temperatures to a definition of the structure in a more "spinodal decomposition"-type fashion. In addition, the observation of a somewhat enhanced interconnectivity for lower quench temperatures is in accordance with the considered pattern of a more "spinodal decomposition"-type of structure for a lower quench temperature.

Additional factors, especially those related to viscosity, might also affect final morphology. For example, for polymer/solvent/nonsolvent ternaries at a lower temperature, the so-called T_T line moves toward compositions of lower polymer content. The crossing of the T_T line is widely considered[42] to lead to the arrest of liquid–liquid demixing phenomena during coagulation employed in versions of the phase inversion technique, though it is possible that the T_T line does not always constitute an insurmountable barrier.[43] In any case, enhanced viscosities (encountered in the case of lower bath temperatures) might fix the polymer-rich phase (and, in consequence, the porous structure as well) at an earlier stage; this might also lead to smaller main pores (possibly with a reduced main porosity and pore contours exhibiting somewhat more crooked contours upon drying). However, we cannot distinguish unequivocally on the basis of the microstructural observations the viscosity-related contributions to membrane porosity features from the more "spinodal decomposition"-like contributions considered earlier in this subsection.

Dope Immersion in Cold Neat Solvent: A New Membrane Fabrication Option. A particularly interesting case was observed when *neat* FA at 10°C was employed as the precipitation medium, i.e., the bath was a cold version of the solvent used in the dope.

The resulting morphology is shown in Figure 7(a,b). This PA12 membrane exhibits a very uniform cross section, and it is composed of crystalline particles having a more or less spherical shape, while there is no evidence for cellular pores. In Figure 7(c), the cross-polarized cross-polarized micrograph (POM) micrograph of Figure 7(a) is demonstrated. Here, the bright spots are indicative of the presence of crystallinity in the solid domains; membrane crystallinity is quantified in the next section by XRD and DSC means. Compared to the microstructure obtained via application of the TIPS method [Figure 7(d)], the particles here [Figure 7(b))] are much smaller ($\sim$1.5 μm), less compact, and have a rather porous surface composed of irregular twisted lamellae; similar structures have been reported previously to derive from polymer crystallization.[15,17,36,44] In the case of TIPS application, crystallization is caused by heat transfer, which destabilizes the single-phase dope. In the present immersion case, both heat and mass transfer will take place; when the dope solution contacts the bath, FA will undergo exchange at the interface due to chemical potential differences in these two regions. Dilution of the membrane solution is expected if influx of FA from the bath prevails over outflux from the casting solution. Less concentrated dopes tend to lead to membranes with smaller crystalline particles; the latter tendency was attributed to viscosity reasons.[37,45] Based on the morphologies of the membranes shown in Figure 7(a,b), it can be inferred that substantial dilution of the casting solution has occurred during the corresponding precipitation process, though the details of the

Applied Polymer SCIENCE

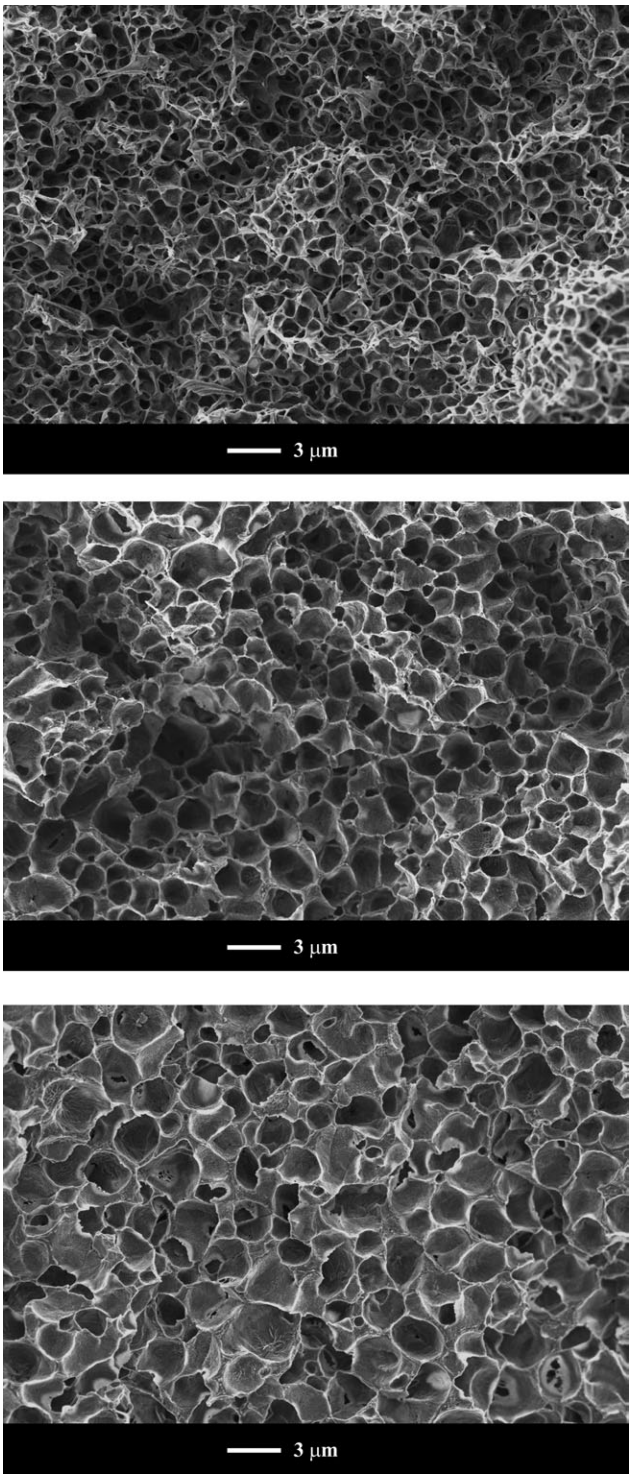

Figure 6. Cross-sectional morphologies of the PA12 membrane. Dope: 20 wt % PA12 in FA. Bath: 90 wt % FA at (a) 10°C, (b) 25°C, and (c) 40°C.

mechanism are complicated, and they are currently investigated further. In addition, it is necessary to optimize this novel membrane fabrication mode, as the membranes obtained so far are mechanically weaker than those obtained by TNIPS (see below). Nevertheless, the fact that it is possible to prepare porous membranes having structures differing from those obtainable either by TIPS or via coagulation in usual precipitation baths is intriguing as regards structural options. In addition, the practical significance of this new and potentially widely applicable membrane fabrication option should not escape attention. The employed membrane-forming system consists only of a polymer and its solvent, and hence, the precipitation bath can be used repeatedly, as opposed to the nonsolvent–solvent–polymer membrane-forming systems, for which the maintenance of a stable bath composition is always a difficult yet crucial, for reproducible structural outcomes, task.

XRD and DSC Analyses of the Membranes

In Figure 8, X-ray diffraction patterns of some typical membranes are shown. The characteristic peak of the γ-type crystal structure at the 21.4° (001) plane can be identified.[36,39,46] This confirms the occurrence of crystallization during the phase demixing process. The diffraction pattern can be decomposed into amorphous and crystalline regions by a curve fitting technique.[15,23] For example, the decomposed diffractogram of the membrane "MW-10" is shown in Figure 8, and from this analysis, the crystallinity of the membrane was determined to be approximately 37%.[47] The crystallinities of the remaining membranes were determined in the same way, and the results are listed in Table II. We find that all membranes exhibit a similar level of crystallinity despite their difference in porous structure.[23,31] This finding need not reflect closely related crystallization conditions; it might be ultimately a reflection of the glass transition temperature being not-far from room temperature (e.g., $T_T = 45$°C for a RH = 50%[47]) of PA12, while small molecules present in the membrane-forming mass before drying further enhance chain mobility. As a result, regardless of case-specific crystallization details for each type of membrane, PA12 will have the opportunity/time to adopt a pseudo-equilibrium crystallinity value that is typical of polymer's molecular weight, while the exact details of solidification amount collectively to factors of secondary importance. The limited range of crystallinity values reported even for compact PA12 (typical: 0.3, after annealing at 150°C: 0.35–0.40[48]) is compatible with this interpretation.

The melting temperature of PA12 crystals in various membranes was determined by means of DSC thermal analysis for three representative membrane samples. Figure 9 shows the melting endotherms obtained for a scanning rate of 10°C/min. All thermograms exhibit a major melting peak and also a lower temperature secondary peak (or shoulder) that corresponds to the melting of small, less stable crystalline units. The measured major melting peak temperatures (T_T), as summarized in Table II, are all close to 179°C, a value typical of PA12 polymer determined by thermal analysis.[26,47] The DSC-based crystallinity of the samples was obtained on the basis of the determined heat of fusion (ΔH_H) and the $\Delta H^0 = 233.6$ J/g literature value for perfect crystalline PA12.[25,26] Although the double peaks in the thermograms are compatible with an irreversible melting process involving recrystallization, the calculated crystallinities, as presented in Table II, are largely in agreement with the results from XRD measurements. This implies that either the level of recrystallization during thermal analysis was low or the heat absorbed during recrystallization was compensated by the heat released during melting of the formed crystals.

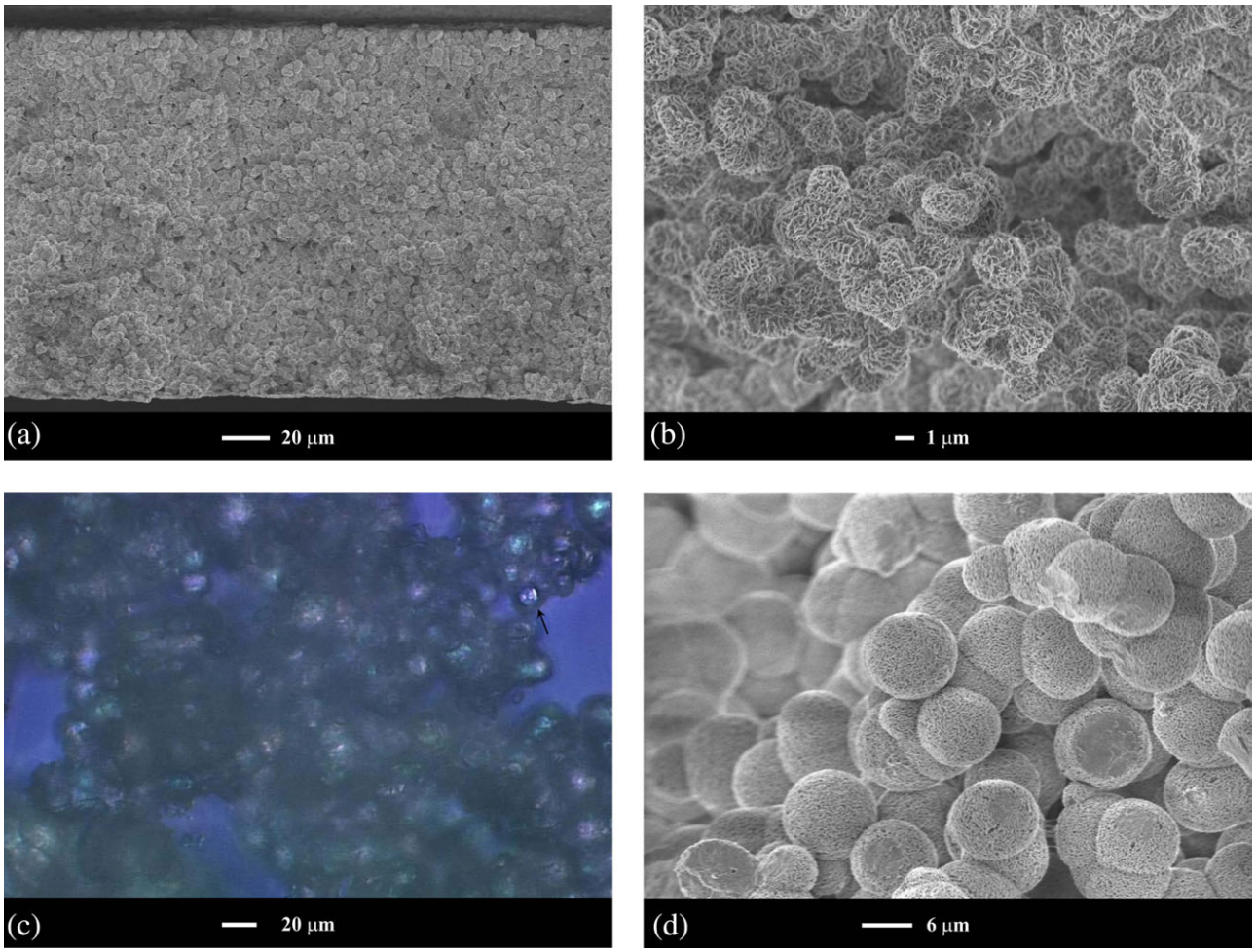

Figure 7. Cross-sectional morphology of the PA12 membrane formed by (a) immersing a 20 wt % dope in pure FA bath at 10°C, (b) high magnification of (a), (c) cross-polarized POM micrograph of (a), and (d) TIPS method. [Color figure can be viewed in the online issue, which is available at wileyonlinelibrary.com.]

Tensile Strengths and Water Flux of the PA12 Membranes

The water fluxes (LMH, L/m^2 h) of various membranes were determined under a transmembrane pressure of 40 or 392 kPa. The results are listed in Table I, in which each point represents the average value of three experimental runs. For the membrane series MW, M30, M50, M70, M80, and M90, the water flux could not be obtained even when pressure was raised to 392 kPa. Obviously, the low water flux for these membranes is associated with the presence of the dense skin and the limited extent of structural bi-continuity (despite the substantial level of porosity), features which effectively impede the permeation of water through the membrane. The water flux of the membrane M95 is very small and is measurable only for high transmembrane pressures (392 kPa). In contrast, the membrane MFA-10 exhibits acceptable flux for a pressure level (40 kPa) appropriate for microfiltration applications. For the un-skinned membranes, the pore sizes, determined by the bubble-point method, are as follows: MFA-10 = 8.51 μm, M95-25 = 1.81 μm, M95-10 = 0.72 μm, and M95-40 = 0.434 μm. While undoubtedly morphological differences contribute substantially to the relative level of water fluxes, comparison of the determined pore sizes

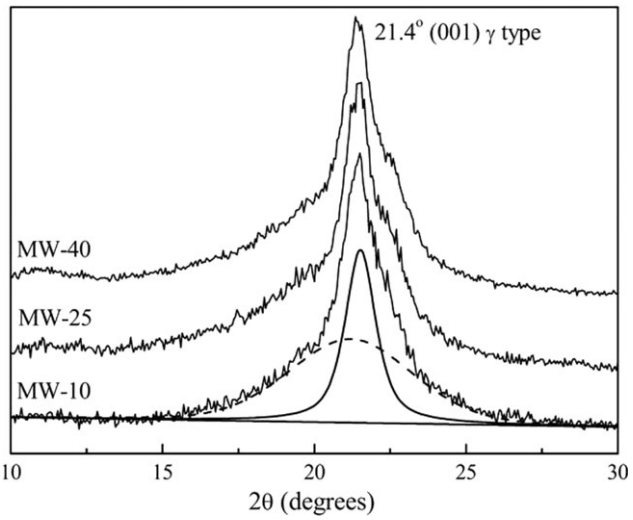

Figure 8. XRD diffractograms of PA12 membranes prepared by immersion-precipitation in water bath at different temperatures. Amorphous and crystalline regions being sorted by curve fitting technique for the MW-10. - - -: amorphous region.

Table II. Thermal Properties and Crystallinity of PA12 Membranes

Bath	Bath temp. (°C)	T_T (°C)	ΔH of PA12 (J/g)	Crystallinity (%)[a]	Crystallinity (%)[b]
Water	10	179.91	87.59	37.5	37.2
	25	178.84	87.73	37.6	37.5
	40	179.20	90.42	38.7	37.1
30 wt % FA	10	180.41	88.14	37.7	38.2
	25	179.26	88.74	38.0	37.6
	40	179.71	92.60	39.6	38.3
50 wt % FA	10	179.83	86.78	37.1	37.2
	25	179.48	87.56	37.5	37.9
	40	179.03	93.77	40.1	38.1
70 wt % FA	10	180.81	86.43	37.0	37.2
	25	178.94	90.33	38.7	38.3
	40	178.87	94.70	40.5	37.9
80 wt % FA	10	180.98	94.36	40.4	38.2
	25	179.80	93.56	40.1	38.5
	40	179.59	92.96	39.8	37.8
90 wt % FA	10	178.98	98.39	42.1	37.6
	25	179.19	100.2	42.9	38.2
	40	177.01	100.8	43.2	38.4
95 wt % FA	10	180.82	97.73	41.8	38.4
	25	180.93	101.7	43.5	37.9
	40	177.47	101.8	43.6	38.3
FA	10	180.33	102.6	43.9	38.4
	25[c]	179.47	109.6	46.9	39.1
	40[c]	180.19	122.5	52.4	39.6

[a] $\Delta H^0 = 233.6$ J/g.
[b] Amorphous and crystalline regions being sorted by curve fitting technique.
[c] Polymer powder; no coherent membrane was obtained when the *neat* FA bath was kept at 25°C or 40°C.

with the fluxes reported in Table I shows a water flux–pore size trend: water flux drops, as pore size drops.

The tensile strengths at break of various membranes are listed in Table III. The average values from five experimental runs are reported together with deviations. The presence of skin and also the level of porosity and degree of crystallinity of the bulk[49] all affect the level of tensile strength; in addition, *fine* morphological differences can easily lead to substantially different strength values even if none of the aforementioned parameters is strikingly different; for example, in the case of globular morphologies, the quality of interglobular connections can easily have a very strong effect on the strength of the globule assembly of the membrane.

For the membrane MFA, which are skinless and highly porous, the tensile strength was 1.8 MPa. The membranes MW, M30, M50, M70, M80, and M90 are all very strong with tensile strength as high as 8.5–13.6 MPa, a range which is only a few times lower than that for the compact polymer (showing strengths typically in the range of 50–60 MPa). The presence of skin and the robust polymer framework morphology of the bulk contribute to the enhanced strength.

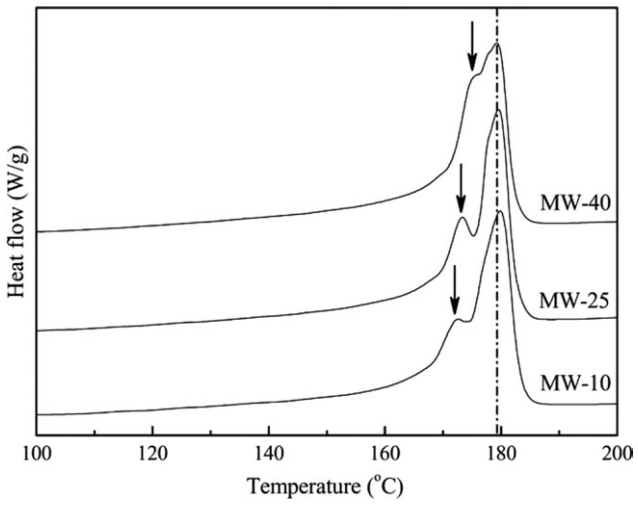

Figure 9. DSC thermograms of PA12 membranes prepared by immersion-precipitation in water bath at different temperatures.

Table III. Tensile Strengths of Membranes Precipitated from Different Baths

Bath	Bath temp. (°C)	Average elongation (%)	Average tensile force (kg)	Average thickness (μm)	Average tensility (MPa)[a]
Water	10	1.11	1.10	133 ± 3	11.6
	25	1.82	1.21	133 ± 7	12.7
	40	1.18	1.40	151 ± 3	13.0
30 wt % FA	10	1.44	1.16	147 ± 6	11.0
	25	1.83	1.34	138 ± 5	13.6
	40	1.03	1.20	147 ± 8	11.5
50 wt % FA	10	1.54	1.27	146 ± 4	12.2
	25	1.72	1.32	151 ± 2	12.3
	40	1.67	1.34	144 ± 5	13.0
70 wt % FA	10	1.08	1.05	134 ± 4	11.0
	25	1.28	1.09	143 ± 4	10.7
	40	1.11	1.06	143 ± 5	10.4
80 wt % FA	10	1.31	0.98	132 ± 3	10.4
	25	1.32	1.16	140 ± 1	11.6
	40	1.04	1.33	147 ± 4	12.7
90 wt % FA	10	1.32	0.93	153 ± 6	8.5
	25	0.71	0.93	149 ± 3	8.8
	40	0.97	0.98	147 ± 2	9.3
95 wt % FA	10	1.13	0.75	164 ± 4	6.4
	25	0.99	0.70	165 ± 3	5.9
	40	1.18	1.03	156 ± 2	9.2
FA	10	0.47	0.21	164 ± 6	1.8
	25[b]	-	-	-	-
	40[b]	-	-	-	-

[a]Tensile strength at break.
[b]Polymer powder; no coherent membrane was obtained when the *neat* FA bath was kept at 25°C or 40°C.

CONCLUSIONS

PA12, which is an attractive engineering polymer in compact form, is found appropriate for the development of porous membranes with both asymmetric and symmetric structures via a combined thermal and nonsolvent phase inversion technique. It is found that some of the porous structures for common polyamide (such as PA6 and PA66) membranes are also possible for the more polyolefin-like polyamide. Asymmetric membranes exhibit much higher tensile strengths than the symmetric membrane due to the presence of a dense top surface and a cellular cross section. They are, however, found to be water-impermeable over the pressure range of 40–392 kPa, except for the case of precipitation in very concentrated (95%) FA bath. Furthermore, dope coagulation via immersion in a cold solvent bath, a novel variation of the phase inversion technique, is considered briefly. Skinless porous membranes are formed, which exhibit an interesting microstructure, composed of interlinked globular spherulites. This membrane demonstrates reasonably high water flux at the transmembrane pressure of 40 kPa for microfiltration process.

ACKNOWLEDGMENTS

The authors thank the National Science Council of Taiwan for the financial support (NSC 96-2628-E-032-001-MY3).

REFERENCES

1. Brydson, J. In Plastics Materials, 7th ed.; Butterworth Heinmann: Oxford, **1999**; Chapter 18.
2. Roh, S. C.; Park, M. J.; Yoo, S. H.; Kim, C. K. J. *Membr. Sci.* **2012**, *411*, 201.
3. Tao, H. J.; Xia, Q.; Chen, S. J.; Zhang, J.; Wang, X. L. *Desalin. Water Treat.* **2010**, *17*, 294.
4. Vanegas, M. E.; Quijada, R.; Serafini, D. *Polymer* **2009**, *50*, 2081.
5. Song, Z. Y.; Xing, M. H.; Zhang, J.; Li, B. A.; Wang, S. C. *Sep. Purif. Technol.* **2012**, *90*, 221.
6. Shibutani, T.; Kitaura, T.; Ohmukai, Y.; Maruyama, T.; Nakatsuka, S.; Watabe, T.; Matsuyama, H. J. *Membr. Sci.* **2011**, *376*, 102.
7. Lloyd, D. R.; Atkinson, P. M. J. *Membr. Sci.* **2000**, *175*, 225.
8. Lloyd, D. R.; Matsuyama, H.; Berghmans, S. *Polymer* **1999**, *40*, 2289.
9. Li, X. L.; Zhu, L. P.; Zhu, B. K.; Xu, Y. Y. *Sep. Purif. Technol.* **2011**, *83*, 66.

10. Buonomenna, M. G.; Golemme, G.; Choi, S. H.; Jansen, J. C.; De Santo, M. P.; Drioli, E. *Sep. Purif. Technol.* **2011**, *77*, 104.
11. Thakur, B. K.; De, S. *Sep. Purif. Technol.* **2012**, *93*, 67.
12. Rahbari-Sisakht, M.; Ismail, A. F.; Matsuura, T. *Sep. Purif. Technol.* **2012**, *86*, 215.
13. Liu, F.; Hashim, N. A.; Liu, Y. T.; Abed, M. R. M.; Li, K. *J. Membr. Sci.* **2011**, *375*, 1.
14. vandeWitte, P.; Dijkstra, P. J.; vandenBerg, J. W. A.; Feijen, J. J. *Membr. Sci.* **1996**, *117*, 1.
15. Cheng, L. P.; Lin, D. J.; Chang, C. L.; Lee, C. K. *Eur. Polym. J.* **2006**, *42*, 356.
16. Cheng, L. P.; Dwan, A. H.; Gryte, C. C. *J. Polym. Sci. Pol. Phys.* **1995**, *33*, 211.
17. Cheng, L. P.; Shih, C. H.; Gryte, C. C. *J. Appl. Polym. Sci.* **2005**, *96*, 944.
18. Yave, W.; Quijada, R.; Serafini, D.; Lloyd, D. R. *J. Membr. Sci.* **2005**, *263*, 146.
19. Yang, Z. S.; Li, P. L.; Xie, L. X.; Wang, Z.; Wang, S. C. *Desalination* **2006**, *192*, 168.
20. Matsuyama, H.; Maki, T.; Teramoto, M.; Asano, K. *J. Membr. Sci.* **2002**, *204*, 323.
21. Tanaka, T.; Nishimoto, T.; Tsukamoto, K.; Yoshida, M.; Kouya, T.; Taniguchi, M.; Lloyd, D. R. *J. Membr. Sci.* **2012**, *396*, 101.
22. Matsuyama, H.; Takida, Y.; Maki, T.; Teramoto, M. *Polymer* **2002**, *43*, 5243.
23. Cheng, L. P.; Lin, D. J.; Chang, H. H.; Chen, T. C.; Lee, Y. C. *Eur. Polym. J.* **2006**, *42*, 1581.
24. Cheng, L. P. *Macromolecules* **1999**, *32*, 6668.
25. Asadinezhad, A.; Jafari, S. H.; Khonakdar, H. A.; Bohme, F.; Hassler, R.; Haussler, L. J. *Appl. Polym. Sci.* **2007**, *106*, 1964.
26. Rhee, S.; White, J. L. *J. Polym. Sci. Pol. Phys.* **2002**, *40*, 1189.
27. Van Krevelen, D. W. Properties of Polymers; Elsevier Science Press: London, **1997**.
28. Tsai, H. A.; Ruaan, R. C.; Wang, D. M.; Lai, J. Y. *J. Appl. Polym. Sci.* **2002**, *86*, 166.
29. Yoon, L. K.; Kim, B. K. *J. Appl. Polym. Sci.* **2000**, *78*, 1374.
30. Mulder, M. Basic Principles of Membrane Technology; Kluwer Academic: Dordrecht/Boston/London, **1991**.
31. Chang, H. H.; Yao, L. C.; Lin, D. J.; Cheng, L. P. *Sep. Purif. Technol.* **2010**, *72*, 156.
32. Kuo, C. Y.; Lin, H. N.; Tsai, H. A.; Wang, D. M.; Lai, J. Y. *Desalination* **2008**, *233*, 40.
33. Young, T. H.; Cheng, L. P.; Lin, D. J.; Fane, L.; Chuang, W. Y. *Polymer* **1999**, *40*, 5315.
34. Shang, M. X.; Matsuyama, H.; Maki, T.; Teramoto, M.; Lloyd, D. R. *J. Appl. Polym. Sci.* **2003**, *87*, 853.
35. Vadalia, H. C.; Lee, H. K.; Myerson, A. S.; Levon, K. *J. Membr. Sci.* **1994**, *89*, 37.
36. Lloyd, D. R.; Kinzer, K. E.; Tseng, H. S. *J. Membr. Sci.* **1990**, *52*, 239.
37. Matsuyama, H.; Iwatani, T.; Kitamura, Y.; Tearamoto, M.; Sugoh, N. J. *Appl. Polym. Sci.* **2001**, *79*, 2449.
38. Matsuyama, H.; Yuasa, M.; Kitamura, Y.; Teramoto, M.; Lloyd, D. R. *J. Membr. Sci.* **2000**, *179*, 91.
39. Cheng, L. P.; Young, T. H.; You, W. M. *J. Membr. Sci.* **1998**, *145*, 77.
40. Haasen, P., Ed. Materials Science and Technology, Volume 5: Transformations in Materials; VCH Publ.: Weinheim, **1990**; Chapter 7 (by K. Binder).
41. Huston, E. L.; Cahn, J. W.; Hilliard, J. E. *Acta Metall. Mater.* **1966**, *14*, 1053.
42. Li, S. G.; vandenBoomgaard, T.; Smolders, C. A.; Strathmann, H. *Macromolecules* **1996**, *29*, 2053.
43. Beltsios, K. G.; Bedard, M. C. M. *J. Macromol. Sci. Phys. B* **2000**, *39*, 623.
44. Aubert, J. H. *Macromolecules* **1988**, *21*, 3468.
45. Shang, M.; Matsuyama, H.; Maki, T.; Teramoto, M.; Lloyd, D. R. *J. Polym. Sci. Pol. Phys.* **2003**, *41*, 194.
46. Phang, I. Y.; Liu, T. X.; Mohamed, A.; Pramoda, K. P.; Chen, L.; Shen, L.; Chow, S. Y.; He, C. B.; Lu, X. H.; Hu, X. *Polym. Int.* **2005**, *54*, 456.
47. Bhattacharyya, A. R.; Bose, S.; Kulkarni, A. R.; Potschke, P.; Haussler, L.; Fischer, D.; Jehnichen, D. *J. Appl. Polym. Sci.* **2007**, *106*, 345.
48. Mark, J. E., Ed., Polymer Data Handbook; Oxford University Press: Oxford, **1999**.
49. Lin, D. J.; Chang, H. H.; Beltsios, K.; Don, T. M.; Jeng, Y. S.; Cheng, L. P. *J. Polym. Sci. Pol. Phys.* **2009**, *47*, 1880.